Advanced GPU-Based Terahertz Approach for In-Line Multilayer Thickness Measurements

Soufiene Krimi, Garik Torosyan, and René Beigang

(Invited Paper)

***Abstract*—In this contribution, an advanced numerical regression approach based on graphics processing unit is introduced. The approach has been applied for real-time terahertz thickness measurements of individual layers within multilayered structures for a variety of industrial applications, including automotive paints, and ceramic coatings. In order to increase the sensitivity and the accuracy of the thickness measurements, a self-calibration method is presented, which can be applied for simultaneous material parameters extraction of all layers from the sample at its final state, taking into consideration all effects that may occur during the coating process.**

***Index Terms*—Thickness measurements, terahertz, multilayer, automotive paints, ceramic coatings, inline, thin films, quality control, calibration.**

I. Introduction

TERAHERTZ (THz) is, in principle, a unit of frequency equal to one trillion hertz (10^{12} Hz). In the last two decades, this term refers often to the region of the electromagnetic spectrum from about 100 GHz to 10 THz, corresponding to wavelengths from 3 mm to 30 μm in vacuum. Terahertz waves lie between the microwave and infrared regions. The boundaries between these regions are not strictly defined, and highly depend on such aspects as generation and detection methods. This band of the electromagnetic spectrum, known until recently as 'THz gap', has been almost technically inaccessible because of the lack of efficient sources and detectors. The first THz-time-domain spectrometer was successfully demonstrated in the late 1980s by Grischkowsky and his colleagues [1]. Terahertz waves combine the benefits of the two neighboring frequency ranges. Unlike infrared, terahertz penetrates a wide variety of non-conductive materials and on the other hand exhibits a better spatial resolution than microwaves. Furthermore, terahertz photons are in contrary to the high-energy x-ray photons non-ionizing and, therefore, are not harmful for living tissue or humans. Research in the terahertz range has seen rapid progress in a short time. This involves, on the one hand, the development of new or further optimization of existing THz generation and detection methods, devices, and systems. On the other hand the investigations relating to the potential of terahertz waves in many new commercial applications. Indeed, defense and security applications are the most discussed research fields of terahertz radiation, including the so-called body scanners [2], explosives and drugs detection [3]–[5], and mail screening [6]. Different hazardous materials have unique spectral 'fingerprints' in the terahertz range. The absorption features are a unique and distinct signature of a wide field of dangerous substances even when they are obscured by clothing or other non-conductive materials. Terahertz technology has opened up also new opportunities in studies of biological tissues, genetic analysis, and cancer diagnosis as well as in the analysis of DNA signatures and protein structures due to their promising properties e.g. their low photon energy [7]–[10]. Moreover, the difference of hydration levels in human body provides good contrast for soft tissue because, as well known, polar substances like water show strong absorption at terahertz frequencies [11]. Another research field of terahertz waves is the wireless sub-THz and THz communication. It has attracted a great deal of interest due to the inherently higher bandwidth of terahertz radiation compared to millimeter waves. The broad bandwidth of terahertz can be used to achieve enormous transmission data rates [12], [13]. Furthermore, terahertz radiation has been shown to be a suitable and very powerful technique for non-destructive testing and material characterization across a wide band of fields, including the determination of various properties of semiconductors [14], [15], and the quality control of multi-layered materials such as plastic, ceramic, paper, paint, and pharmaceutical tablets, which are transparent in the THz range [16]–[19].

A. Motivation of Terahertz Thickness Measurements

Why is a new technology for thickness measurement needed when other methods have been successfully applied for years with cost-effective commercial devices?

Even if several cost-effective methods are available, the field of multilayer coating quality monitoring and thickness measurement is still an attractive topic, since the industrially used materials for coatings and substrates are continuously improved and optimized in cost and quality. One of the most important developments, in recent years, is the growing use of carbon fiber

Manuscript received October 21, 2016; revised December 5, 2016; accepted December 6, 2016. Date of publication December 29, 2016; date of current version March 2, 2017.

S. Krimi and R. Beigang are with the Department of Physics, Technische Universitat Kaiserslautern, Kaiserslautern 67663, Germany (e-mail: k.soufiene@yahoo.de; beigang@physik.uni-kl.de).

G. Torosyan is with the Photonic Center Kaiserslautern, Kaiserslautern 67663, Germany (e-mail: torosyan@physik.uni-kl.de).

Color versions of one or more of the figures in this paper are available online at http://ieeexplore.ieee.org.

Digital Object Identifier 10.1109/JSTQE.2016.2646520

reinforced polymers instead of the usual metallic substrates in many fields, such as aerospace and automobile constructions. The inherent nature of such substrates related to the conductivity limits the direct use of eddy current methods, magnetic induction methods, and in some cases also the ultrasonic method for coating measurements. Furthermore, a typical setup of automotive paint system consists of up to four layers, including the electrocoat, the filler, the basecoat, and the clearcoat. A full quality control requires measuring the paint thickness of the individual layers. The photo thermal approach as well as the eddy current method, and the magnetic induction method are only able to measure the total thickness of a multi-layered structure. The individual layers cannot be resolved with these techniques. Because of these constraints, techniques that can measure the individual layer thickness of both single and multilayer systems are advantageous for such measurement applications. Ultrasonic approaches, based on sound waves, can resolve the individual layers in a multilayer structure. However, this technology often requires a coupling gel to couple the ultrasonic wave in the material and, thus, is not suitable to be applied for wet paints. A great potential to overcome these restrictions has been introduced by the terahertz technology, which combines the benefits of the conventional techniques. The unique properties of terahertz waves to penetrate non-conductive materials, to be reflected at each interface between two layers of optically different materials, and to measure a back reflection from the substrate surface for both metallic and non-metallic substrates, make this new technology to an alternative approach with great potential.

B. State of the Art in Terahertz Thickness Measurements Research

The fact that the terahertz spectrum lies between the microwave and the infrared regimes offers the possibility to generate and detect terahertz radiation by either electronic or optical methods which include both coherent and incoherent approaches. Coherent systems can be roughly divided into two techniques depending on the spectrum of the generated terahertz radiation: pulsed terahertz waves which are characterized by a large bandwidth (typically over 3 THz) and continuous terahertz waves within a narrow frequency spectrum (typically a bandwidth of a few GHz). The feasibility of thickness measurement using coherent continuous wave (CW) or coherent pulsed terahertz systems has been investigated in the last few years by several research groups. Electronic continuous wave photomixing terahertz systems are increasingly being applied for single layer and multilayer thickness measurement because of their lower cost, small size, and high frequency resolution in the order of a few MHz. These systems are, however, mostly limited by the 2π ambiguity of previous continuous wave signals and their low frequency tuning range. Meanwhile, new multi-wavelength CW-systems which are able to circumvent the 2π uncertainty and capable of measuring multilayer thickness are presented [20]–[22]. The measurement time for such systems depends on the frequency tuning range, which currently amounts up to a few minutes for a broadband signal. Yet, the measurement time of multi-wavelength CW-systems for a broadband signal prevents actually the application of such approaches for inline process control of thin layers such as automotive paint coatings. Pulsed terahertz technique using a femtosecond laser offers, however, a broad frequency signal with a high dynamic range in a short measuring time in the order of few milliseconds. Because of these properties, pulsed terahertz techniques are, currently, still preferred for inline thin film thickness measurement, where a broadband signal is required. A high-resolution time-of-flight terahertz spectrometer was introduced on 2009 by J Takayanagi et al., which combined optical pulses compressed to 17 fs using optical fibers and a DAST crystal. They have generated and detected broadband terahertz pulses ranging from 0.1 to 27 THz. Using deconvolution signal processing, the wideband spectrum of the generated terahertz waves provided high-axial resolution leading to successful imaging of a multilayered structure containing a 2-μm-thin GaAs layer [24]. Generally, commercial THz systems use photo-conductive antennas. They provide useful signals from 0.1 THz up to 5 THz. The attainable bandwidth is influenced predominantly by the laser pulse duration, which has a typical duration of about 100 fs. The minimum measurable thin layer thickness using terahertz technique is related to the terahertz system specifications, including bandwidth and dynamic range as well as the evaluation approach of the measured data. A direct determination of the layer thickness can be performed from the time delay between two successive pulse echoes from the front and back surfaces of the coating. However, it is limited by the terahertz pulse length and the refractive index of the investigated coating. The limit of a direct determination of coating layer with a refractive index of 1.5 using a terahertz system with a pulse length of 0.8 ps is estimated to be about 80 μm. For thinner layers, the pulse echoes, which describe the boundaries of the single layers within a layered structure, overlap in the time domain so that their time separation cannot be determined precisely. In order to decrease the limit of the minimum measurable thickness, a variety of numerical fitting methods and optimization algorithms to separate overlapping subpulses was proposed recently. One of the first remarkable approaches in this field was published on 2007 by Yasuda *et al.* [25]. They propose a multiple regression analysis approach using the least-square fitting algorithm in order to decrease the minimum paint film thickness for THz spectrometers. The used model neglected the multiple reflections effect within the multilayer structure, the absorption, and the dispersion of the individual coatings. Nevertheless, the model showed the great potential of THz technology by decreasing the minimum measurable film thickness from 108 μm down to 20 μm. Recently, Su *et al.* [26] extended the numerical parameter fitting method proposed by Yasui et al. by integrating the etalon effect, the absorption and dispersion of material in the simulation algorithm. However, they continue to use a deterministic least-square fitting algorithm to determine the thicknesses. Furthermore, they approximate the refractive index to be constant and the absorption coefficient to be linear over the frequency range under consideration. Using the proposed approach, the minimum thickness was decreased down to 18 μm for both single and multilayer automobile paints [26]. A second very interesting approach to investigate multilayer coatings using TDS-reflection and

transmission geometries was suggested recently by van Mechelen *et al.* [31]. The presented method treats the investigated structure as a stratified system and for each layer extracts the material properties using a suitable dispersion model, such as the Lorentz-model. Very similar to the method presented by Yasui *et al.* and Zeitler *et al.*, van Mechelen et al. use a time domain fitting procedure based on a least-squares algorithm. In order to enhance the accuracy of the proposed analysis method, a time-domain and frequency-domain fitting procedure has been applied simultaneously. The main benefit of this model is the use of a stratified dispersive model, which reduces the number of sought variables significantly, enabling a simultaneous extraction of the individual optical material parameters in multilayer structures. The existing approaches have been successfully applied for paper samples and multilayer automotive paints for thicknesses down to 18 μm.

To summarize these approaches, it has to be noted that the evaluation algorithms are an important core for the study of thin films using THz spectroscopy. Such algorithms usually consist of three main steps:

1) *Calibration:* it refers to the extraction of the spectral optical material parameters of each single layer based on either the classical inverse TDS-model or a suitable approximation using for example a dispersive model.
2) *Simulation:* it refers to the mathematical modeling of the THz waves propagation within the investigated multilayer structure based on the already calculated optical material parameters from the calibration step and a set of initial values of thickness for the entire layers.
3) *Optimization:* here, the thicknesses of individual layers are frequently varied until an optimum correlation between the measured and the simulated pulse is achieved, which corresponds to the numerical determination of the correct thicknesses.

C. Principle of Thickness Measurements

Terahertz technique is a non-destructive contactless technology. When a pulse of terahertz radiation encounters an interface between two media of different optical material parameters, it is partly reflected and partly transmitted. The same phenomena is repeated at each interface. The time delay between two reflected echoes from two adjacent boundaries corresponds to the optical thickness. For optically thick samples, the reflected adjacent echoes are well separated in time domain so that the individual thicknesses can be calculated directly from the time delay Δt_z based on time-of-flight as follows:

$$d_z = \frac{c\Delta t_z}{2n_z \cos\theta_z}, \tag{1}$$

where θ_z is the angle of incidence and n_z is the refractive index. For thin films, the pulse echoes, which describe the boundaries of the single layers within the multilayer system, overlap in the time domain so that their time separation cannot be determined precisely. In order to resolve the thicknesses of the individual layers, a numerical regression approach has to be applied.

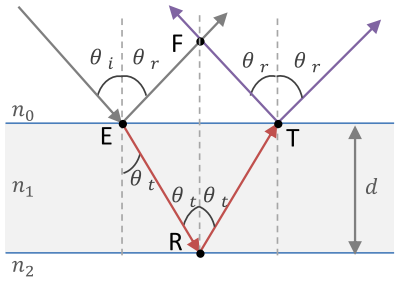

Fig. 1. The optical path length difference of a thin film.

II. Thin Films

A. Definition

At least in the terahertz range, the definition of a thin film is not strictly defined. A general definition defines the boundary between thick and thin films at 100 μm [29], [30]. This value can be taken as an absolute geometrical thickness or as an optical path, which has to be divided from the refractive index. A second definition describes with the term "thin films" any layer whose main reflected pulse and the multiple reflected pulses partially overlap in time domain [27], [28], [32]. This definition stems from the increasing complexity in the data evaluation process. The coating thickness measurement of these thin films, where the individual reflections interfere constructively or destructively, can not be calculated directly from the signal time delay. For such applications, a theoretical model is required to simulate the terahertz pulse in the time domain. In order to achieve an accurate film thickness measurement, the simulation model must fulfill the following criteria. It should:

1) be suitable for the characterization of thin films in the THz range.
2) be applicable for an arbitrary number of layers.
3) take into consideration all possible occurring main reflections and multiple reflections within the investigated multilayer structure.
4) be applicable for arbitrary polarizations and angles of incidence.
5) take into account the dispersion and the absorption of the materials under test.
6) provide a fast computation time, which is typically within a range of few milliseconds in order to perform in-line measurements.

B. Effective Thickness of Thin Films

In the evaluation of measurement data at oblique beam incidence, it is important to note that the effective layer thickness does not correspond to the geometrical layer thickness. For thick layers, the effective thickness can be calculated directly as a division of the geometrical thickness by the cosine of the transmitted angle:

$$d_{eff} = \frac{d}{\cos\theta_t}. \tag{2}$$

For thin layers, the interference effects must be taken into account. As shown in Fig. 1, the new effective thickness is the path

that the pulse passes through the layer until the interference with the other partial waves.

Mathematically, this path difference can be expressed in the following way. The geometric path difference of the reflected waves at the points E and R in Fig. 1 is:

$$\overline{ER} + \overline{RT} - \overline{EF} = 2\overline{ER} - \overline{EF}, \tag{3}$$

where

$$\overline{ER} = \frac{d}{\cos\theta_t},\ \overline{EF} = \overline{ET}\sin\theta_i,\ \overline{ET} = 2d\tan\theta_t. \tag{4}$$

By combining (3) and (4), we get:

$$2\overline{ER} - \overline{EF} = \frac{2d}{\cos\theta_t} - 2d\frac{n_1}{n_0}\tan\theta_t\sin\theta_t. \tag{5}$$

To obtain the optical path difference, we multiply $\overline{EF}$ with the refractive index n_0 and $\overline{ER}$ with the refractive index n_1:

$$\frac{2dn_1}{\cos\theta_t} - 2dn_1\tan\theta_t\sin\theta_t = 2dn_1\cos\theta_t. \tag{6}$$

Hence, the effective thickness at oblique incidence is:

$$d_{eff} = d\cos\theta_t. \tag{7}$$

C. Numerical Modeling of Terahertz Waves Propagation in Multilayer Thin Films

From the field of system theory, it is known that the output signal of any system results from the convolution between the input signal and the impulse response in the time domain. In this sense, a multilayer coating is nothing else than a system which produces a reflected and a transmitted radiation from an incident wave. The signal processing can also be performed in the frequency domain, where the convolution operation can be simplified to multiplication of the Fourier transform of the impulse response (known also as the transfer function $H(\omega)$) and the Fourier transform of the incident THz pulse $E_i(\omega)$:

$$E_r(\omega) = E_i(\omega)H(\omega), \tag{8}$$

Equation (8) indicates that the modeling of an arbitrary coating system with known incident pulse, also here referred to reference pulse, corresponds to the calculation of its transfer function.

1) Single Layers: Fig. 2 shows a schematic representation of the wave interaction with a single layer at oblique incidence.

The transfer function of a single coating layer in reflection can be derived from the sum of the main reflections and the multiple reflections within the layer as follows:

$$H(\omega) = r_{01} + \frac{t_{01}t_{10}r_{12}e^{\frac{2i\widetilde{n}\omega d}{c}}}{1 - r_{10}r_{12}e^{\frac{2i\widetilde{n}\omega d}{c}}}, \tag{9}$$

where the terms d, $\widetilde{n}$, t_{ab} and r_{ab} denote the thickness value, the complex spectral refractive index, the Fresnel reflection coefficient and the Fresnel transmission coefficient between two media a and b, respectively.

2) Multi-Layered Thin Films: To derive an analytical formula for a multilayer coating in reflexion, the individual reflected partial sub-waves can be summed up according to amplitudes and phases in similar manner as for the case of a single layer. However, the wave behavior is more complicated with an increasing number of layers because the multiple reflections of the individual layers can propagate over several layers and cause again multiple reflections. An elegant approach to simulate the wave propagation within an arbitrary multilayer structure can be described by either the transfer matrix method or the Rouard's Method.

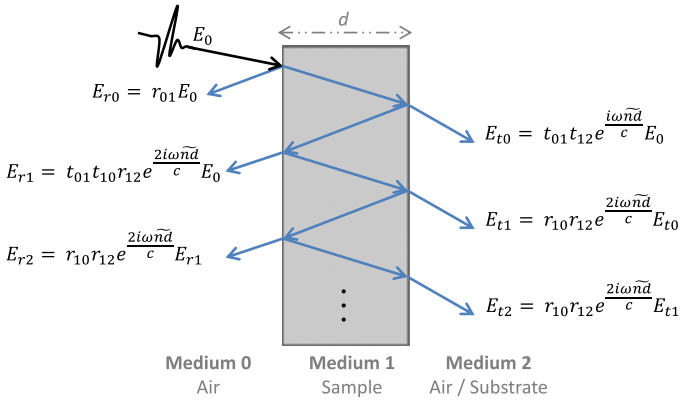

Fig. 2. Schematic representation of a THz wave interaction with a single layer at oblique incidence, including the reflected and transmitted signal.

The transfer matrix method, abbreviated as TMM, is a widely used model to calculate the total reflectance and total transmittance of thin film structures. It is a powerful tool because it provides high computational accuracy for simultaneous modeling of transmissivity and reflectivity, a fast computing time, and it is easily programmable [33], [34]. The method models each layer with two 2×2-matrices: $D_{l,l+1}$ and P_l. The $D_{l,l+1}$-matrix represents the behavior of the terahertz pulse at each interface between two media with different optical material constants, containing the corresponding Fresnel coefficients

$$D_{l,l+1} = \frac{1}{t_{l,l+1}}\begin{bmatrix} 1 & r_{l,l+1} \\ r_{l,l+1} & 1 \end{bmatrix}, \tag{10}$$

where $t_{l,l+1}$, and $r_{l,l+1}$ are the Fresnel transmission coefficient and the Fresnel reflection coefficient, respectively. The propagation of the terahertz signal within the layer and hence its phase change is modeled with the propagation matrix P_l

$$P_l(\omega) = \begin{bmatrix} e^{i\omega\widetilde{n}_l d_l} & 0 \\ 0 & e^{-i\omega\widetilde{n}_l d_l} \end{bmatrix}. \tag{11}$$

The two matrices can be reduced to a 2×2-matrix M_l:

$$M_l = P_l.D_{l,l+1} = \frac{1}{t_{l,l+1}}\begin{bmatrix} e^{i\omega\widetilde{n}d} & r_{l,l+1}e^{i\omega\widetilde{n}d} \\ r_{l,l+1}e^{-i\omega\widetilde{n}d} & e^{-i\omega\widetilde{n}d} \end{bmatrix}. \tag{12}$$

The entire behavior of a multilayer thin film structure is then obtained by multiplying all layers' matrices M_l

$$M^{total} = \prod_{l=0}^{N} M_l = \prod_{l=0}^{N} P_l.D_{l,l+1} = \begin{bmatrix} M_{11} & M_{12} \\ M_{21} & M_{22} \end{bmatrix}. \tag{13}$$

Here, N denotes the number of layers in the investigated structure. From M^{total}, the reflectance and the transmittance of a multilayer structure can be calculated directly and simultaneously. In the case of reflection, the transfer function is given

by

$$H_R(\omega) = \frac{M_{21}(\omega)}{M_{11}(\omega)}. \tag{14}$$

In the case of transmission, it is expressed as

$$H_T(\omega) = \frac{1}{M_{11}(\omega)}. \tag{15}$$

A second suitable method to model multilayer structures was published for the first time in 1937 by Rouard [35], [36]. The model is a recursive process which works similar to the transfer matrix method. In contrast to TMM, the Rouard's method is able only to calculate either the transmittance or the reflectance. For the explanation of this model, let us take into account only the first coating that is deposited onto the substrate. The modeling process starts from this layer, which is first considered as a single layer with a simple transfer function $H_l(\omega)$

$$H_l(\omega) = r_{l-1,l} + \frac{t_{l-1,l}t_{l,l-1}r_{l,l+1}e^{\frac{2i\tilde{n}_l\omega d_l}{c}}}{1 - r_{l,l-1}r_{l,l+1}e^{\frac{2i\tilde{n}_l\omega d_l}{c}}}, \tag{16}$$

where l denotes the layer index, d_l is the coating thickness, n_l is the complex spectral refractive index, c is the speed of light in vacuum, $t_{l,l+1}$, and $r_{l,l+1}$ are the Fresnel transmission coefficient and the Fresnel reflection coefficient, respectively. Now, we interpret the overlying layer $l-1$ again as a single layer with the simple transfer function like the previous layer l

$$H_{l-1}(\omega) = r_{l-2,l-1} + \frac{t_{l-2,l-1}t_{l-1,l-2}\boldsymbol{r_{l-1,l}}e^{i\beta}}{1 - r_{l-1,l-2}\boldsymbol{r_{l-1,l}}e^{i\beta}}, \tag{17}$$

where $\beta = \frac{2\tilde{n}_{l-1}\omega d_{l-1}}{c}$. So far, the two layers are interpreted as simple single layers. The idea of Rouard is to replace the Fresnel reflection coefficient in (17) with the complete transfer function of the adjacent layer l. So we integrate the entire effects together, which provides a full description of the multilayer structure. The transfer function of a two-layer sample using the Rouard's method is then given by

$$H^2_{Total}(\omega) = r_{l-2,l-1} + \frac{t_{l-2,l-1}t_{l-1,l-2}\boldsymbol{H_l(\omega)}e^{i\beta}}{1 - r_{l-1,l-2}\boldsymbol{H_l(\omega)}e^{i\beta}}. \tag{18}$$

For an arbitrary number of layers, it is necessary to "follow the path back" from the substrate to the incident medium, finding the total reflection coefficient at each interface in turn.

D. Comparison of Modeling Methods

The TMM and Rouard's method are two suitable approaches for modeling multilayer structures in the THz range. The computing speed of both methods is calculated theoretically for multilayer structures with a different number of layers based on a MATLAB implementation on CPU. The computing times for a number of layers varying between 1 and 6 are plotted in Fig. 3.

The Rouard's method is for one simulation, depending on the number of layers, up to 8 ms faster than the transfer matrix method. The two models are also compared based on highly parallelized GPU codes. An important factor for the parallelization performance is the allocated memory for the modeling method, which may include information such as allowed maximum number of parallel simulations and computation time. Fig. 4 illustrates the allocated memory by the GPU compiler by increasing number of simulations.

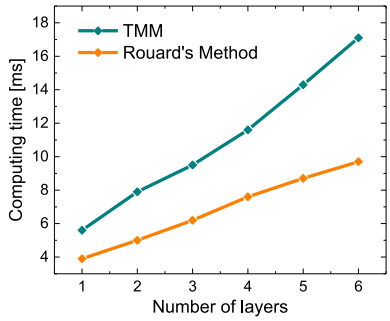

Fig. 3. Graphical representation of the computation times for the TMM and the Rouard's method

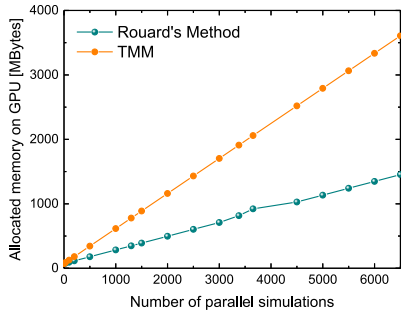

Fig. 4. Comparison of the measured allocated GPU memory for the Transfer matrix method and Rouard's method with increasing number of simulations.

It can be observed that the TMM needs significantly more GPU memory than the Rouard's method. The transfer matrix method and the Rouard's method are both powerful approaches for modeling multilayer structures. However, the Rouard's method outperforms the transfer matrix method by a faster computation time and a lower memory allocation. In this contribution, the Rouard's method is selected as a simulation method.

III. Optimization

We can distinguish between two types of optimization algorithms: deterministic and stochastic, also known as meta-heuristic or evolutionary algorithms. The deterministic approach, such as the simplex method, the gradient method, and the Newton's method are powerful tools for local minima search and for specific optimization problems with known gradient matrices and Hessian matrices, which determine the optimum direction and distance of the search after each iteration, increasing the optimization efficiency. The advantage of such methods is the rapid and precise procedure. For complex search spaces with several local minima, deterministic methods are not efficient because they depend very strongly on initial values. Once a local minimum is reached, the algorithm can not continue to search the global minimum. In contrast, stochastic optimization methods are increasingly applied for practical problems because they provide many benefits compared to deterministic methods. They are based on randomness, statistics, and probability, which

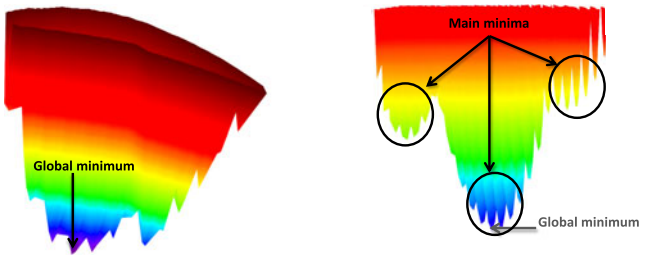

Fig. 5. (left) Mean square error distribution for a three-layer specimen. (right) Mean square error distribution for a four-layer specimen.

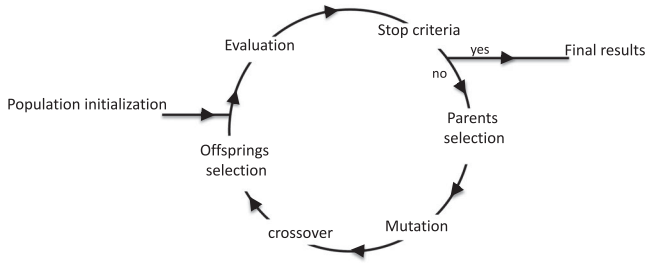

Fig. 6. Schematic flowchart for evolutionary algorithms process.

increase the probability to find the global minimum, even for objective functions that are non-differentiable, non-continous, non-linear, noisy, multi-dimensional or have a complex search space with several local minima. The most known algorithms in this class comprise genetic algorithms (GA), developed by John Holland in the 1960s and 1970s [37]; differential evolution (DE), introduced by Storn and Price in 1997 [38]; adaptive simulated annealing (ASA), introduced by Metropolis et al. in 1953 [39] and particle swarm optimization (PSO), introduced by Kennedy and Eberhart in 1995 [40]. Experience with terahertz thickness measurement has shown that several local minima exist in the search space. As illustrated in Fig. 5, complex cases can be clearly seen in the case of three-layer samples and four-layer samples. The figure illustrates a typical mean square error distribution in the search space. The color blue indicates a better correlation between measurement and simulation than the color red.

The search space for the four-layer specimen consists of three main minima, including two local minima and a global minimum. Each of the three main minima consists again of several local minima. In this case, an efficient algorithm must be able to jump out of all these local minima and to achieve the desired results. In order to increase the probability to find the best solution, even for thin layers with a complex search space, an evolutionary stochastic algorithm is used instead of the deterministic algorithms.

A. Evolutionary Optimization Algorithms

Evolutionary algorithms (EAs) are population-based approaches, which aim to mimic the theory of natural evolution through the "survival of the fittest" principle: fittest solution candidates have higher survival chances to the next generation than the weaker ones. Evolutionary algorithms realize this concept through three main mathematical operators: mutation, recombination, and selection. As shown in Fig. 6, the interchange between these three operations continues iteratively until a termination condition is met [41], [42].

The differential evolution algorithm (DE) operates using a set of candidate solutions, also known as population. Each candidate solution in the population, known as an individual, includes four real-valued numbers, presenting the thicknesses of the individual coatings. The real-valued thickness numbers are often called genes. The fitness of the individuals is given by the value of the mean square error between the simulated and measured data.

1) Population Initialization: The first step in the optimization process is the initialization of the population. Each thickness value of each individual in the initial population is randomly generated within a predefined search space based on the following formula:

$$d_{i,j}^{initial} = lb_i + rand(0,1) \times (ub_i - lb_i)\,, \tag{19}$$

where $rand(0,1)$ is a single uniformly distributed random number between 0 and 1, j is the individual index, lb_i, and ub_i are the lower and upper thickness bounds of the layer i, respectively.

2) Mutation: The differential algorithm derived its name from the differential mutation operator. The DE approach differs from other evolutionary algorithms mainly in the mutation operator, which generates randomly new populations from the old ones based on a vector addition, multiplication and subtraction between the old individuals. In this work, we use the "DE/rand/1" mutation scheme [38]

$$M_j = P_{r_1} + F * (P_{r_2} - P_{r_3}), \tag{20}$$

The mutation is applied for each population candidate in current population (parents) P_j to generate mutated individuals in an intermediate population M_j.

3) Recombination (Crossover): The crossover operator is an essential complementary step to mutation, which recombines the parents P_j with the intermediate mutated individuals M_j to produce an offspring population O_j. Here, the binomial variant has been used, which can be represented by the following formula:

$$O_j = \begin{cases} M_j & \text{if } rand_j(0,1) \le CR, \\ P_j & \text{otherwise.} \end{cases} \tag{21}$$

Here, j denotes the individual index and $rand(0,1)$ is a single uniformly distributed random number in the interval (0, 1). The parameter CR determines the probability that an offspring individual is taken from the mutated population.

4) selection: The aim of the selection operator is that only the fittest candidates from the parent and offspring populations of the current generation survive to the next generation. It means that an offspring individual replaces a parent individual in the next generation if it has a better fitness value. Otherwise, the parent individual is retained.

5) Stop Criteria: After the selection step, a new generation of parent population is created, which in turn passes through the entire process from mutation to selection. This procedure is repeated until a specified stop criterion is satisfied. An important step for the efficiency of any optimization is the termination criterion. The user has to select an appropriate criterion to terminate the optimization process as soon as the global mini-

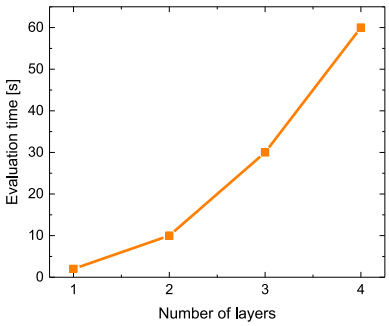

Fig. 7. The optimization time increases exponentially with increasing number of layers.

mum is reached. An efficient criterion is to terminate the process when the change of the best individuals or of the object function from one iteration to the next is less than a predetermined tolerance value.

B. Challenges for In-Line Data Evaluation

Differential Evolution is a powerful approach to solve complex optimization problems. However, it evaluates all individuals in a population for every generation in each optimization step, including mutation, crossover, and selection. Thus, the evaluation time can take from a few seconds to a few hours due to the high demanding computing needs, depending on the dimension and complexity of the problem. Despite its efficiency, the long computation time prevents its use in many industrial applications. Fig. 7 shows the calculated evaluation time based on a MATLAB implementation running on a processor with eight cores.

Firstly, an exponential curve can be seen, which reflects the complexity of the search space with an increasing number of layers. An in-line measurement system for the industrial applications usually requires an evaluation time below one second. As shown in Fig. 7, the computing time already exceeds the 1 second-limit with the evaluation of two layers. To overcome this drawback, a parallel implementation of such algorithms using FPGAs or GPUs can enhance their performance.

IV. GPU-Based Model for In-Line Sensing

The field of parallel computing deals mainly with processing of large data volumes, which often requires intensive computation. Its main purpose is either to enhance the processing time for complex tasks or to solve very large computational problems, operating on the principle that large data can be evaluated simultaneously as a set of small portions. Here, the term accelerators refers to special purpose processors developed for massively parallel high-performance computing [43]. Two popular accelerator devices are the field programmable gate arrays (FPGAs) and the graphics processing units (GPUs), which often enhance the performance compared to CPUs. R. Brodtkorb *et al.* [44] present the state of the art in parallel computing by comparing the performance of FPGA and GPU. In a second work [43], Che et al. also compare the performance of GPUs, FPGAs and multi-core CPUs in parallel computing. They both come to the conclusion that FPGAs as well as GPUs are powerful devices

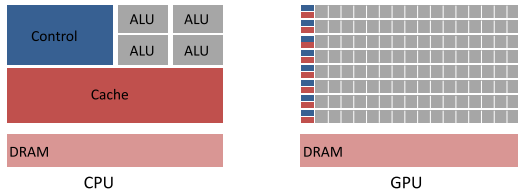

Fig. 8. A schematic comparison of resource allocation in CPUs and GPUs [45].

for high performance applications. Furthermore, they concluded that FPGAs have the charm of compact size, lower power consumption, and highly customizable architecture. However for large data volumes, FPGAs often require more hardware resources than GPUs. Thus, the complexity of development for the architectures of FPGAs in terms of time and cost is higher than for a GPU with similar properties. This contribution focuses on NVIDIA GPUs in combination with the programming language C-CUDA used in our experimental implementations.

A. GPU Computing and CUDA Architecture

1) GPU Computing: Graphics Processing Units (GPUs) are multi-core programmable processors on a graphics card. Traditionally, a GPU is used as an accelerator for 3D computer graphics, such as 3D games. Meanwhile, GPUs have evolved into a highly parallel, multithreaded environment with exceptional parallel computational power. The reason why GPUs offer so much more performance than modern CPUs lies essentially in the different architectures. As schematically illustrated in Fig. 8, the design of a GPU is fundamentally different from the arrangement of a CPU.

CPUs are characterized by large caches to minimize memory access latency, a large area for control logic to optimize the execution of sequential code, and a comparatively small number of arithmetic-logic units (ALU). These resource distributions in a CPU are not designed for the execution of multiple parallel instructions, but for an optimal and efficient execution of serial tasks. Conversely, the graphics processors consist of several hundreds of cores enabling them to run thousands of threads in parallel. A large area for the control logic and the cache is therefore not required. This enables a GPU to solve compute-intensive problems. However, for inherently not parallelizable tasks, CPU is outperforming GPUs since CPUs have typically faster clock frequencies.

2) CUDA Architecture: General-purpose computing on graphics processing units (GPGPU) refers to the utilization of a graphics processing unit to enhance computation performance in a variety of academic and industrial applications. In 2007, NVIDIA designed its Compute Unified Device Architecture (CUDA) as part of its parallel computing architecture. NVIDIA also released a programming language, called C-CUDA, which facilitates the access to the available resources and the programming of the single units. C-CUDA is an extension of the C programming language. The sources distribution in a CUDA architecture is illustrated in Fig. 9. In CUDA environment, the terms "host" and "device" denote the CPU and the GPU, respectively. The CUDA architecture is built around a programmable array of multithreaded streaming multiprocessors (SM). Each multi-

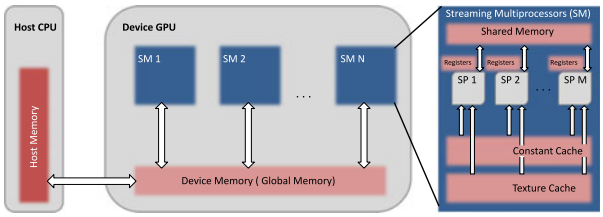

Fig. 9. Schematic representation of CUDA architecture [45].

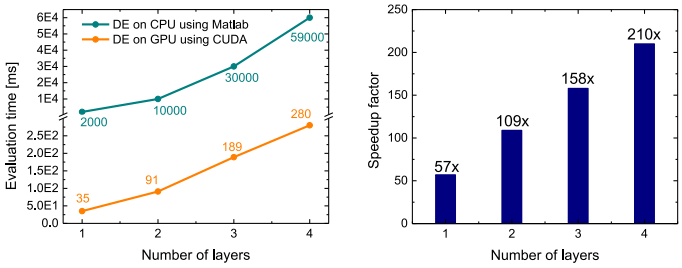

Fig. 10. A comparison between the DE performance on CPU and GPU. (left): the evaluation time, (right) the speedup factor.

processor contains several single processors (SP), also known as cuda cores, which can execute a large amount of threads on parallel. The global device memory is accessible to all single processors and provides direct communication between host and device to transfer the data in both directions. The data transfer between host and device is the slowest process. Therefore, the amount of data transferred between CPU and GPU has to be minimized and optimized to improve the computing speed. On the other hand, shared memory, registers, texture, and constant memory are accessible to all threads within the same multiprocessors (SM). Hence, a synchronization between the single threads is therefore necessary in order to avoid access conflicts. The number of cuda cores on chip depends on the architecture but is constant for all SMs in the device.

B. GPU-Based Optimization

The aim of the DE implementation by a CUDA environment is achieving high parallelism while retaining the simplicity and the global search benefits of the algorithm. DE is an iterative process that executes the individual operators sequentially, including population initialization, crossover, mutation, evaluation, and selection. These steps are therefore not parallelizable because each operator needs the results of the previous step. Fortunately, the most time and processor consuming task is the objective function calculation, which operates in a highly parallel way. Figure shows the evaluation time of the highly parallelized algorithm on a GPU compared to the MATLAB implementation on a CPU. As illustrated in Fig. 10, we were able to successfully achieve a computation time below 1 second for four-layer samples. This corresponds to an acceleration of **210** times compared to the CPU implementation. It is also to see that the speedup factor increases with increasing number of layers. This is expected because the increasing number of layers provides more parallelization potential. The evaluation time of the highly parallelized algorithm is below 300 ms when investigating a four-layer sample. Hence, the industrial

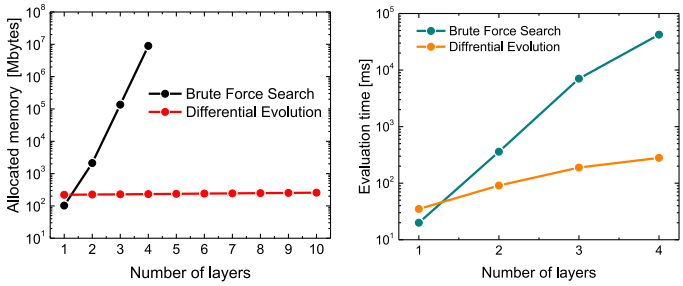

Fig. 11. A comparison between the performance of DE and brute force search on GPU. (left): the allocated memory, (right): the evaluation time.

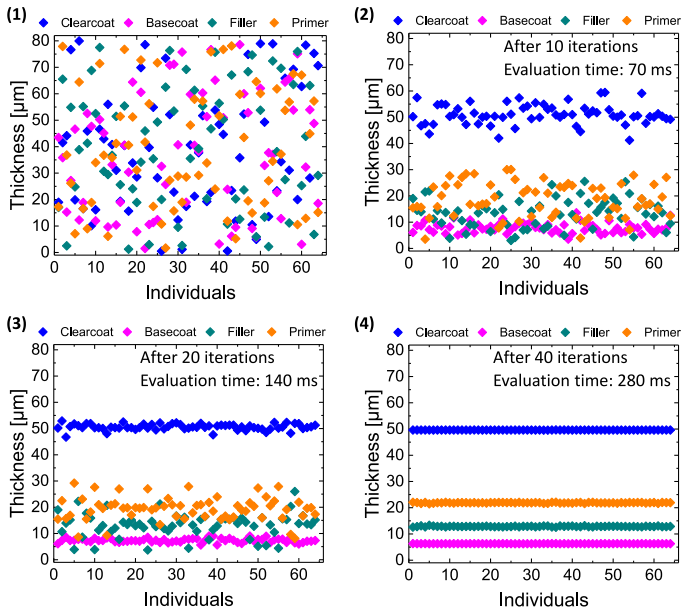

Fig. 12. The operation of the GPU-based algorithm inside the optimization loop for a four-layer automotive paint specimen.

requirements for inline measurement systems are fulfilled. Besides the fast computation time, the developed algorithm is also characterized by low memory usage. As sketched in Fig. 11, DE needs approximately 220 MB for a single layer. With each additional layer, DE allocates only additional 4 MB. In contrast, the Brute-Force search needs only 120 MB for a single layer which increases exponentially with the number of layers so that the required memory to investigate a four-layer sample amounts about 8 TB. Therefore, the brute force search shows a little faster computation time than DE for single layers. However, the DE is **153** times faster when investigating four-layer samples. For these results, DE is also more accurate than brute force as it uses floating point numbers while brute force uses only integer values for the thicknesses. An example of the operation of the DE algorithm on GPU is shown in Fig. 12. The presented sample is a simulation for a four-layer automotive paint specimen, including primer, filler, basecoat, and clearcoat.

In the first figure, the start population is initialized with random values between 0 μm and 80 μm for each layer. The iterations are repeated until the termination criterion occurs. The second and third figures show the effect of mutation, crossover, and selection operators, which pass the fittest solution candidates and eliminate the weaker ones after each iteration.

TABLE I
TYPICAL THICKNESS VALUES FOR THIN COATINGS

Layer	Thickness value
zinc phosphate	3 μm–8 μm
Electro-coat	16 μm–23 μm
Primer	20 μm–35 μm
Basecoat	5 μm–35 μm
Clearcoat	40 μm–60 μm

The clearcoat and basecoat show a faster convergence behavior than primer and filler due to their better contrast, which is described by the spectral refractive index and the spectral absorption index. In the fourth figure, it can be nicely observed how all individuals of the last population converge to the same global minimum after 40 iterations, which corresponds to a processing time of only 280 ms. The deviation of all individuals lies well below 1 μm giving a direct information about the accuracy of the algorithm.

V. THICKNESS MEASUREMENT USING THZ-TDS: APPLICATIONS AND RESOLUTION

The results are generated using a compact fiber-coupled spectrometer "T-Spectralyzer" (Hübner GmbH & Co. KG, Kassel, Germany) with a transceiver device and compared with conventional measurement methods such as eddy current.

A. Automotive Paint Industry

Vehicle paint quality control in the automotive and aircraft industry is one of the promising industrial applications of terahertz technology since most applied coatings are transparent for terahertz radiation. The purposes of the painting process in the manufacturing hierarchy are to protect the vehicle body against corrosion, scratching, and weathering as well as to provide an attractive appearance to the vehicles. In order to fulfill these targets optimally, the optimum quantity of paint must be applied. The paint may not provide a long life protection if less than the desired quantity is applied. On the other hand, coating materials are also expensive. Paint overspray leads to unnecessary waste and disposal costs. The painting process is a complex multistep process where five layers of thin coatings, including zinc phosphate, e-coat, primer or filler, basecoat, and clearcoat, are deposited on the vehicle surface. Typical thicknesses values for the five layers are given in Table I.

The zinc phosphate coating is a conductive material which reflects the terahertz signal on its surface completely. Therefore, the reflected THz signal provides only information about the thicknesses of the subsequent coatings, including e-coat, primer, basecoat, and clearcoat. A typical THz pulse form for such applications as well as the overlapping principle of the individual reflections are sketched in Fig. 13.

The target in such cases is to extract the individual thicknesses even after the constructive and destructive overlap, which is possible due to the highly accurate regression process.

1) Calibration: The first step is the calibration which deals with the extraction of the complex refractive index of all layers

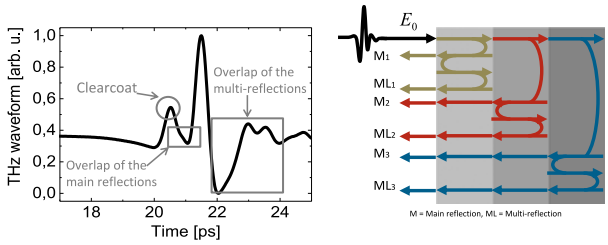

Fig. 13. A typical THz pulse form for the automotive paints (left) and the principle of multiple overlapping individual reflections (right).

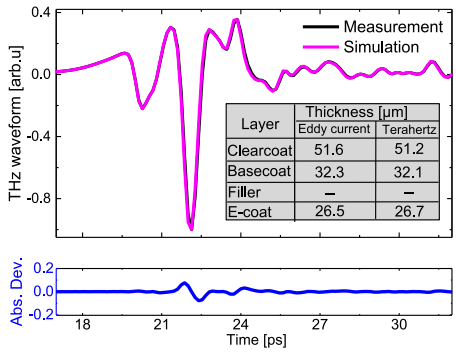

Fig. 14. A comparison between measurement and simulation of a three-layer paint sample on a metallic substrate. The analysis is optimized using the self-calibrating approach and the stochastic optimization. For comparison, the individual layer thickness are determined using an eddy current device on a step-wedge. The abbreviation "'Abs. Dev.'" denotes the absolute deviation between measurement and simulation.

in the investigated sample. In a widely used classical calibration method, the individual coatings of a multilayered sample have been first applied as single layers on metallic substrates. Their thicknesses are determined using an alternative nondestructive technique e.g. eddy current. Next, the spectral refractive indices and the extinction coefficients are analyzed in reflection mode in advance. This model assumes that the material parameters do not change later in the multilayer system during the production process. However, a wet-on-wet spray takes place in the painting process. Consequently, the adjacent layers partly merge causing a change of the material parameters compared to the single layers. To overcome this problem, a self-calibration approach is developed, which is applied during the production process. This self-calibration model can be applied to extract the material parameters of all layers from the sample at its final state, simultaneously. Hence, we take into consideration all effects that may occur during the paint process such as wet-on-wet spray. The idea is to use dispersion models or simple approximations such as the linear fit to extract the material parameters. Thus, we reduce the number of unknowns making the system of equations mathematically solvable.

Several automotive paint samples with different colors have been investigated based on the developed approach. The basecoats can be roughly divided into solid or glossy. Glossy basecoats include either aluminum flakes or special iridescent pigments to impart the car more brilliance while solid basecoats provide no optical effects except the color.

2) Three-Layer Paint Samples on Metallic Substrate: Fig. 14 illustrates the results obtained for a three-layer automotive paint

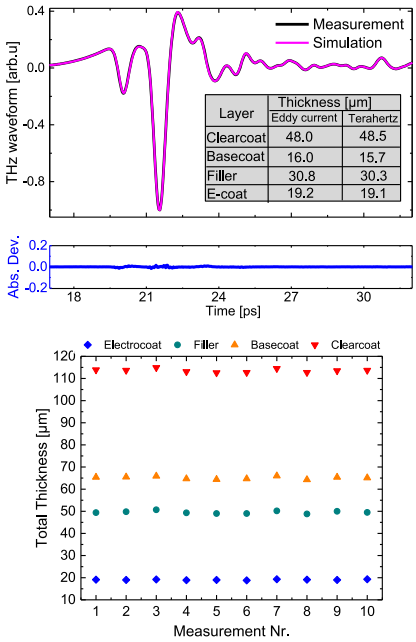

Fig. 15. A comparison between measurement and simulation of a four-layer paint sample on a metallic substrate. For comparison, the rated values for the individual layer thickness are determined using an eddy current device on a step-wedge (top). The scattering of the obtained thickness values for 10 different measurements at the same position (bottom). The abbreviation "'Abs. Dev."' denotes the absolute deviation between measurement and simulation.

sample on metallic substrate. The basecoat color is white. The results have been always compared with alternative techniques to determine the accuracy.

The results obtained after the optimization process show a very good graphical agreement between the measured THz signal and the simulated one. Moreover, the measured values agree nicely with the thicknesses obtained with the eddy current device.

3) Four-Layer Paint Samples on Metallic Substrate: The results of a four-layer paint sample, including an electrocoat, a filler-coating, a metallic silver basecoat containing aluminium flakes and a basecoat are shown in Fig. 15. The measured thicknesses are compared to rated values obtained by an eddy current device. The excellent graphical fit results and the close match of the thickness values demonstrate the robustness of the developed approach. For industrial applications, a deciding benchmark of the performance of a method is the repeatability or precision of the measurements. The repeatability is the more critical factor while accuracy is also important. Fig. 15 also illustrates a scatter plot of the achieved results based on 10 different measurements at the same position. A maximum absolute deviation of 0.5 μm is achieved for the individual layers.

4) Imaging: Besides the in-line thickness monitoring where a point measurement is required, the developed approach can also be applied for online and offline applications where a complete surface control is desired. With the set-up used in these measurements, the measurement time for one point amounts to 1 second. The developed approach provides an evaluation time below 300 ms for a four-layer specimen. The total measurement time of a complete surface depends on the number of the measured pixels. Fig. 16 illustrates an example of a surface measurement on a steel sheet having the dimension 20 cm $\times$ 18 cm. The sample has three paint coatings with double opposite wedges in the clearcoat and the filler.

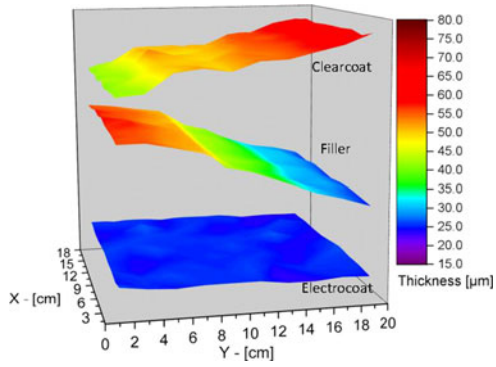

Fig. 16. A 3D thickness image of a three-layer specimen with double opposite wedges in clearcoat and filler.

5) Minimum Thickness Resolution: The minimum thickness resolution is an important issue because many paint coatings in the automotive sector are in the range of 10 μm. Unfortunately, a general lower limit for all types of layers cannot be given since the minimum resolution depends on several parameters such as the specifications of the measurement system, the contrast between the individual layers in the sample, and the thicknesses of the adjacent layers. In this work, the following formula was derived, which can determine the minimum resolution of any individual layer within a multilayer paint sample:

$$d^i_{\min} = \frac{\frac{\Delta T \times c}{2n_i}}{2\left(\frac{n_k d_k}{30} + \Delta n\right)}, \tag{22}$$

where ΔT is the THz pulse duration, i is the index of the investigated layer and n_i its effective refractive index. The term c denotes the light speed in vacuum, n_k, and d_k are the effective refractive index and the thickness of the adjacent layer with lower contrast:

$$n_k, d_k = \begin{cases} n_{i-1}, d_{i-1} & \text{if } |n_{i-1} - n_i| \leq |n_{i+1} - n_i|, \\ n_{i+1}, d_{i+1} & \text{otherwise.} \end{cases} \tag{23}$$

Δn is the absolute value of the refractive index difference between n_i and n_k. The principle of derivation of the equation consists of two main points. The term $(\Delta T \times c)/(2n_i)$ in the numerator determines the boundary between thin and thick layers. For thin layers below this boundary, the individual reflections overlap in the time domain. Nevertheless, as shown in this contribution, the thickness value can be determined using a fitting algorithm. With a suitable algorithm, the minimum resolution is then limited only by the dynamic range of the measurement system and the contrast between the individual layers within the multilayered structure. These two effects are described in the denominator with the terms n_k, d_k, and Δn for the contrast and the constant 30 for the dynamic range. The constant value is determined experimentally. The entire term in the denominator is then multiplied by 2 since the wave propagates twice within the layer in the reflection setup. The derived formula has been compared with experimental results from different samples of paint layers with different parameters. The minimum resolution

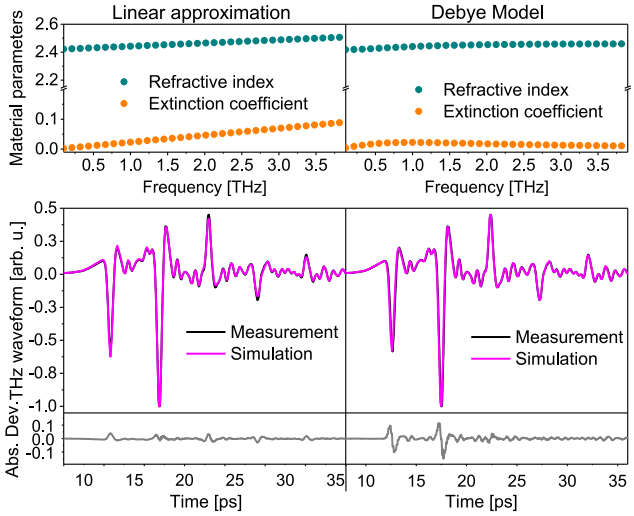

Fig. 17. The extracted material parameters of a ceramic coating using the linear approximation and the Debye Model as well as the corresponding measured and simulated THz-pulses.

can be very well approximated for several samples with different properties and different thickness wedges using the derived formula. The deviation between theory and experiment usually lies below 2 μm.

B. Ceramic Thermal Barrier Coatings (TBCs)

Ceramic thermal barrier coatings (TBCs) are widely used as insulators to protect turbine blades of aircraft engines at temperatures well above 1000 C. The optical material parameters of the specimen under test are usually extracted from a calibration sample, and the thickness values are determined either based on the time delay between two pulse echoes from front and back surfaces of the coating for thick layers or by using a suitable numerical regression approach for thin layers. However, the optical material parameters of TBCs are influenced by the composition of the applied materials, the spraying conditions and the sintering process, resulting in a particular microstructure with varying refractive indices and absorption. The introduced self-calibrating approach is able to extract the spectral optical material parameters of a TBC and determine its thickness value, simultaneously. Furthermore, arbitrary misplacement errors between sample and reference measurements can be corrected. The spectral material parameters can be extracted using a linear approximation or a suitable dispersion model such as the Debye model in order to overcome the ambiguity of the solution. The proposed regression method can be applied in time-domain, frequency-domain or in both the time- and frequency-domain simultaneously. Fig. 17 illustrates an example of the extracted spectral optical material parameters based on the linear dispersion and the Debye model as well as the measured and the simulated THz pulses of a ceramic coating on a metallic substrate.

As can be shown, a good graphical agreement between experimental and simulated data was achieved. Furthermore, the numerical results were compared with the values obtained using an eddy current device. A maximum relative deviation of about 1% is usually achieved.

VI. Conclusion

In summary, we have introduced an advanced regression procedure with a self-calibration model to monitor the quality of multi-layered structures in terms of thickness measurements for a variety of industrial applications, including automotive paints, and ceramic coatings using terahertz technology. The proposed approach combines the benefits of the highly accurate calibration model, an efficient modeling method and the stochastic evolutionary optimization algorithm, taking into consideration the real industrial challenges such as the effect of wet-on-wet spray in the painting process. Using the general-purpose computing on graphics processing units (GPGPU), the computation time is reduced to less than 300 ms. Hence, the every-second-cycle for thickness measurements required from industry is fulfilled. Due to the high robustness of the proposed self-calibration method and the genetic optimization algorithms, the approach has been applied to resolve individual layer thicknesses within multi-layered paint samples well below 10 microns (typically 7 microns) and even down to 4 microns under certain constraints [23]. The absolute accuracy of the achieved results is usually better than 1 μm. For imaging applications, the approach provides a complete surface control.

Acknowledgment

The authors thank Dr. S. Böttger and Dr. T. Weber from Phototherm Dr. Petry GmbH for their kind support. The authors would also like to thank the Hübner GmbH & CO. KG for providing the T-Spectralyzer terahertz measurement system.

References

[1] M. van Exter, C. Fattinger, and D. Grischkowsky, "Terahertz time-domain spectroscopy of water vapor," *Opt. Lett.*, vol. 14, pp. 1128–1130, 1989.

[2] S. Gu, C. Li, X. Gao, Z. Sun, and G. Fang, "Terahertz aperture synthesized imaging with fan-beam scanning for personnel screening," *IEEE Trans. Microw. Theory Tech.*, vol. 60, no. 12, pp. 3877–3885, Dec. 2012.

[3] W. H. Fan *et al.*, "Far-infrared spectroscopic characterization of explosives for security applications using broadband terahertz time-domain spectroscopy," *Appl. Spectrosc.* vol. 61, pp. 638–643, 2007.

[4] L. Ho, M. Pepper, and P. Taday, "Terahertz spectroscopy: Signatures and fingerprints," *Nature Photon.*, vol. 2, pp. 541–543, 2008.

[5] H. B. Liu, Y. Q. Chen, G. J. Bastiaans, and X. C. Zhang, "Detection and identification of explosive RDX by THz diffuse reflection spectroscopy," *Opt. Express 14*, vol. 14, pp. 415–423, 2006.

[6] F. Ellrich *et al.*, "Chemometric tools for analysing terahertz fingerprints in a postscanner," in *Proc. 2012 37th Int. Conf. Infrared, Millim., THz Waves*, 2012, pp. 1–2.

[7] N. Zheng, M. Aghadjani, K. Song, and P. Mazumder, "Metamaterial sensor platforms for terahertz dna sensing," in*Proc. 2013 13th IEEE Conf., Nanotechnol.*,, 2013, pp. 315–320.

[8] M. Wang, G. Yang, W. Li, and Q. Wu, "An overview of cancer treatment by terahertz radiation," in *Proc. 2013 IEEE MTT-S Int. Microw. Workshop Series RF Wireless Technol. Biomed. Healthc. Appl.,*2013, pp. 1–3.

[9] M. He, M. Li, and W. Zhang, "Terahertz time-domain spectroscopy signature of animal tissues," in *Proc. Progress Electromagn. Res. Symp.*, 2008.

[10] D. F. Plusquellic, K. Siegrist, E. J. Heilweil, and O. Esenturk, "Applications of terahertz spectroscopy in biosystems," *Chemphyschem*, vol. 8, pp. 231–241, 2007.

[11] W. Zouaghi, M. D. Thomson, K. Rabia, R. Hahn, and V. B. H. G. Roskos, "Broadband terahertz spectroscopy: Principles, fundamental research and potential for industrial applications," *Eur. J. Phys.*, vol. 34, pp. 179–199, 2013.

[12] S. Hwu, K. deSilva, and C. Jih, "Terahertz (THz) wireless systems for space applications," in *Proc. 2013 IEEE Sens. Appl. Symp.*, Feb. 2013, pp. 171–175.

[13] A. Dogadaev, A. Lavrinenko, and I. Monroy, "Capacity analysis for high-speed terahertz wireless communications," in *Proc. 2012 37th Int. Conf. Infrared, Millim., THz Waves*, Sep. 2012, pp. 1–2.
[14] D. M. Mittleman, J. Cunningham, and M. C. Nuss, "Noncontact semiconductor wafer characterization with the terahertz hall effect," *Appl. Phys. Lett*, vol. 71, 1997, Art. no. 16.
[15] M. van Exter and D. Grischkowsky, "Carrier dynamics of electrons and holes in moderately doped silicon," *Am. Phys. Soc.*, vol. 15, pp. 12140–12149, 1990.
[16] S. Krimi, J. Klier, M. Herrmann, J. Jonuscheit, and R. Beigang, "Inline multilayer thickness sensing by using terahertz time-domain spectroscopy in reflection geometry," in *Proc. 2013 38th Int. Conf. Infrared, Millim., THz Waves*, 2013, pp. 1–2.
[17] L. Owens, M. Bischoff, A. Cooney, D. Petkie, and J. Deibel, "Characterization of ceramic composite materials using terahertz reflection imaging technique," in *Proc. 2011 36th Int. Conf. Infrared, Millim. THz Waves*, 2011, pp. 1–2.
[18] H. Selig, M. Khazan, and I. Wilke, "Optical properties of glasses and ceramics for terahertz-technology," in *Proc. 2000 Conf. Lasers Electro-Optics Eur., 2000. Conf. Digest*, 2000.
[19] Y.-C. Shen and P. Taday, "Development and application of terahertz pulsed imaging for nondestructive inspection of pharmaceutical tablet," *IEEE J. Sel. Topics. Quantum Electron.*, vol. 14, no. 2, pp. 407–415, Mar./Apr. 2008.
[20] M. Scheller, K. Baaske, and M. Koch, "Multifrequency continuous wave terahertz spectroscopy for absolute thickness determination," *Appl. Phys. Lett.*, vol. 96, pp. 151112-1–151112-3, Apr. 2010.
[21] H.-C. Ryu *et al.*, "Simple and cost-effective thickness measurement terahertz system based on a compact 1.55 μm λ/4 phase-shifted dual-mode laser," *Opt. Express*, vol. 20, pp. 25990–25999, 2012.
[22] D. Stanze *et al.*, "Multilayer thickness determination using continuous wave THz spectroscopy," *IEEE Trans. THz Sci. Technol.*, vol. 4, no. 6, pp. 696–701, Nov. 2014.
[23] S. Krimi *et al.*, "Highly accurate thickness measurement of multi-layered automotive paints using terahertz technology," *Appl. Phys. Lett.*, vol. 109, 2016, Art. no. 021105.
[24] J. Takayanagi *et al.*, "High-resolution time-of-flight terahertz tomography using a femtosecond fiber laser,"*Opt. Express*, vol. 17, pp. 7533–7539, Apr. 2009.
[25] T. Yasuda, T. Iwata, T. Araki, and T. Yasui, "Improvement of minimum paint film thickness for THz paint meters by multiple-regression analysis," *Appl. Opt.*, vol. 46, pp. 7518–7526, Oct. 2007.
[26] K. Su, Y. chun Shen, and J. Zeitler, "Terahertz sensor for non-contact thickness and quality measurement of automobile paints of varying complexity," *IEEE Trans. THz Sci. Technol.,* vol. 4, no. 4, pp. 432–439, Jul. 2014.
[27] L. Duvillaret, F. Garet, and J.-L. Coutaz, "A reliable method for extraction of material parameters in terahertz time-domain spectroscopy," *IEEE J. Sel. Topics. Quantum Electron.,* vol. 2, no. 3, pp. 739–746, Sep. 1996.
[28] L. Duvillaret, F. Garet, and J.-L. Coutaz, "Highly precise determination of optical constants and sample thickness in terahertz time-domain spectroscopy," *Appl. Optics*, vol. 38, pp. 409–415, Sep. 1999.
[29] R. Wilk, I. Pupeza, R. Cernat, and M. Koch, "Highly accurate THz time-domain spectroscopy of multilayer structures," *IEEE J. Sel. Topics. Quantum Electron.,* vol. 14, no. 2, pp. 392–398, Mar./Apr. 2008.
[30] M. Scheller, C. Jansen, and M. Koch.,, "Analyzing sub-100-μm samples with transmission terahertz time domain spectroscopy," *Opt. Commun.*, vol. 282, no. 7, pp. 1304–1306, 2009.
[31] J. L. M. van Mechelen, A. B. Kuzmenko, and H. Merbold, "Stratified dispersive model for material characterization using terahertz time-domain spectroscopy," *Opt. Lett.*, vol. 39, pp. 3853–3856, Jul. 2014.
[32] J. O'Hara, W. Withayachumnankul, and I. Al-Naib, "A review on thin-film sensing with terahertz waves," *J. Infrared, Millim., THz Waves*, vol. 33, no. 3, pp. 245–291, 2012.
[33] D. Owens, *Linear and Nonlinear Optical Properties of Metal-Dielectric Multilayer Structures*. Ph.D. thesis, Georgia Inst. Technol., Atlanta, GA, USA, 2010.
[34] E. W. M. Born, *Principles of Optics: Electromagnetic Theory of Propagation, Interference and Diffraction of Light*. Cambridge, U.K.: Cambridge Univ. Press, 1997.
[35] A. Vasicek, "Sur la reflexion de la lumiere sur des verres supportant des couches minces multiples.," *Le J. De Phys. Et Le Radium*, vol. 11, pp. 342–345, Jan. 1950.
[36] A. Vasicek, "Reflexion de la lumiere sur des couches multiples homogenes minces et epaisses," *Le J. De Phys. Et Le Radium*, vol. 12, pp. 590–592, Jan. 1951.
[37] H. J. H, *Adaptation in Natural and Artificial Systems*. Cambridge, MA, USA: MIT Press, 1975.
[38] R. Storn and K. Price, "Differential evolution - A simple and efficient heuristic for global optimization over continuous spaces," *J. Global Optim.*, vol. 11, pp. 341–359, 1997.
[39] N. Metropolis, A. Rosenbluth, M. Rosenbluth, A. Teller, and E. Teller, "Equation of state calculations by fast computing machines," *J. Chem. Phys.*, vol. 21, pp. 1087–1092, 1953.
[40] J. Kennedy and R. Eberhart, *Particle Swarm Optimization*. Piscataway, NJ, USA: IEEE Press, 1995, pp. 1942–1948.
[41] J. Rönkkönen, *Continuous Multimodal Global Optimization With Differential Evolution-Based Methods*. Ph.D. thesis, Acta Universitatis Lappeenranta, Lappeenranta Univ. Technol., Lappeenranta, Finland, 2009.
[42] M. C. du Plessis, *Adaptive Multi-Population Differential Evolution for Dynamic Environments*. Ph.D. thesis, Univ. Pretoria, Pretoria, South Africa, 2012.
[43] S. Che, J. Li, J. Sheaffer, K. Skadron, and J. Lach, "Accelerating compute-intensive applications with GPUS and FPGAS," in *Proc. 2008 Symp. Appl. Specific Process.*, Jun. 2008, pp. 101–107.
[44] A. R. Brodtkorb, C. Dyken, T. R. Hagen, J. M.Hjelmervik, and O. O. Storaasli, "State-of-the-art in heterogeneous computing," *Sci. Program.*, vol. 1, no. 12, pp. 1–33, 2010.
[45] CUDA, "CUDA c Programming Guide, Design Guide," Nvidia Corporation, Santa Clara, CA, USA, Sep. 2015.

Soufiene Krimi received the Graduate Engineering degree in information technology and the Ph.D. degree in electrical engineering from the University of Kaiserslautern, Germany, in 2012 and 2016, respectively. His doctoral research concerned Terahertz thickness measurements of multilayered structures. He is currently a Research Associate in the Ultrafast Photonics and THz Physics Group at the University of Kaiserslautern, Germany. His research interests include industrial applications of Terahertz technology.

Garik Torosyan received the Graduate degree from the Department of radiophysics, Yerevan State University, Armenia. He received the Ph.D. degree from the Institute for Physical Research, Armenian National Academy of Sciences, former USSR, Armenia. The main topic of his research was resonance interaction of ultrashort light pulses with atomic metal vapors. Between 1994 and 1999, parallel to the work in Armenia he has taken part in setting up the activities in the new field of terahertz physics in the group of Prof. R. Beigang at the University of Kaiserslautern Germany. He moved to Germany in 2000 to join the same group as a research member. Now he is a Senior Scientist in the Photonic Center of Kaiserslautern, Kaiserslautern, Germany, and is conducting research on new terahertz components.

René Beigang received the Graduate degree from the University of Hannover, Hannover, Germany. He received the Ph.D. degree from the University of Hannover, Hannover, Germany, in 1979. He received his Habilitation from the Free University of Berlin in 1984 and spent three years as a Heisenberg stipend at the IBM T. J. Watson Research Center in Yorktown Heights. In 1990, he moved to the University in Kaiserslautern, Kaiserslautern, Germany, where he is a Professor in the Department of Physics. His scientific interest started with laser physics, nonlinear optics, and the generation and application of ultrashort pulses in fundamental science and biophysics. From here he moved into the field of generation and application of broadband THz radiation using ultrashort laser pulses in combination with electro-optical methods and nonlinear optics. He contributed to the field of THz metamaterials, time-domain spectroscopy, compact fiber coupled THz systems, and nondestructive testing. During the last 10 years, in particular, applications in an industrial environment were in the focus of his research activities.